JMEPEG (2011) 20:185–190
DOI: 10.1007/s11665-010-9685-2

1059-9495/$19.00

Forming Simulation and Experimental Verification of Combined Formation of Selective Laser Sintering and Cold Isostatic Pressing

Yan Ying Du, Yu Sheng Shi, and Qing Song Wei

(Submitted August 10, 2009; in revised form October 26, 2009)

Selective laser sintering (SLS) could manufacture complex parts rapidly which, however, have high porosity and low intensity. While the parts made by cold isostatic pressing have advantages of uniform structure without composition segregation, high-dimension precision and high density. However, it could not form high complex parts because of the difficulties in manufacturing bag. A combination of SLS and cold isostatic pressing is expected to use the advantages of the two methods and is an efficient way to make complicated parts rapidly. After SLS and cold isostatic pressing, dimensions of parts decrease and relative density increases. To predict final dimensions and density, the finite element simulations are performed for cold isostatic pressing. The results show the parts made from ball shape powder contract symmetrically. The simulation results agree with the achieved geometries within 4%. Comparisons are made with that parts made from irregular powder. The SEM pictures after SLS are also showed. This has an important indication to process of SLS and cold isostatic pressing forming.

Keywords cold isostatic pressing, selective laser sintering, simulation, stainless steel

1. Introduction

Selective laser sintering (SLS) is a rapid prototype technique (Ref 1, 2) and extraordinary complicated parts can be manufactured by SLS. SLS has the advantages of short manufacturing cycle, the ability to form high complex shape parts, and freedom from costly tooling. The parts made by SLS, however, cannot be used for structure components because of the high level of porosity present in the as-processed components. Therefore, the SLSed parts usually are infiltrated by low melting point metal or alloy, such as Cu, bronze, and brass, to fill the pores and improve the intensity. It is obvious that the mechanical properties will be deteriorated by the infiltrated low melting point metal (Ref 3). Selective laser melting (SLM), another rapid prototype technique, can be used to make metal parts. Its scan rate, however, is low and it needs much more time than SLS to make a bigger part. Isostatic pressing (IP) is a near net forming technology and any pores can be closed in the component if they are not surface-connected (Ref 4, 5). Additionally, IP could keep original shape of parts. Therefore, SLS could be combined with IP, and the extent of the porosity could be expected to be reduced. Although this paper used stainless steel powder, this method provides an effective route to manufacture refractory alloy parts. But up to now, the documents about the combination of SLS/IP are seldom. Agarwala et al. (Ref 6) studied manufacturing Ni-bronze parts via SLS and hot isostatic pressing (HIP). They used the glass capsule to densified the rectangular parts in argon state. The technique did not avoid traditional difficulties of capsule producing in HIP process. Liu et al. (Ref 3) manufactured the stainless steel parts by combined SLS/HIP and SLS/CIP/HIP technologies, respectively. The results showed SLS/CIP/HIP technology was a better method to manufacture dense parts than SLS/HIP. The parts made by SLS/CIP/HIP could be pressed into near dense parts with the relative density more than 80% that could be raised if much higher CIP pressure was employed. Ren and coworkers (Ref 7) manufactured stainless steel parts using a combined SLS/CIP technique and studied the dimension deforming in the process. The experiments showed the dimension contraction in one direction is larger and that in other directions is smaller.

This paper is concerned with the combined SLS and CIP forming of stainless steel powder. Unlike Ren, we attempt to use spherical powder to make parts and compare with the results of Ren. The CIP process of SLSed parts is simulated by finite element model to predict the finally dimensions of shaped components. It has been found that there is a general agreement between experiments and predictions.

Yan Ying Du, Yu Sheng Shi, and **Qing Song Wei**, State Key Laboratory of Material Forming and Die and Mould Technology, HuaZhong University of Science and Technology, Wuhan 430074, China. Contact e-mail: jenny_dyy@yahoo.com.cn.

2. Material and Experiments

2.1 The Process of SLS Combined CIP

Water atomized AISI304 stainless steel powder (Beijing Dyna-Veriex Co. Ltd.) with an average particle size of 75 μm was applied in the experiments. The chemical composition of the 304 stainless steel powder is showed in Table 1, and the granularity distribute is shown in Fig. 1. The metal powder has

a regular spherical shape. The mixture of AISI304 powder and epoxy powder was used to manufacture green parts, and they were the matrix material and binder, respectively. The content of epoxy of powder in the mixture was 4 wt.%.

Two kinds of metal green parts which were column shape and brick shape were made by SLS and the green parts formed using a scan route for the laser which is illustrated in Fig. 2. The *X-Y* plane is the build plane, and the *Z* direction is normal to *X-Y* plane and is that of powder accumulation. Then, the low melting point polymer was removed by heating the green parts to about 900 °C in a vacuum furnace. The example samples after SLS are showed in Fig. 3 and 4.

Then, the SLSed parts were dipped into the latex of national rubber for minutes and the rubber were solidified and cross linked at 90 °C for 1 h. The parts coated by the rubber are showed in Fig. 5 with about 2 mm thickness. Then, all the parts were CIPped at 650 MPa.

Table 1 Composition of AISI304 stainless steel powder (w/o)

C	Si	Mn	Cr	Ni	O	P	S	Fe
0.15	0.3	0.6	17.5-18.5	9-10	<0.2	<0.03	<0.02	Balance

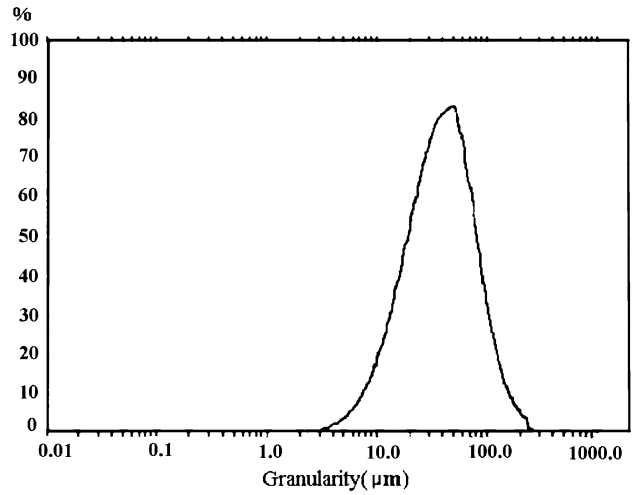

Fig. 1 The granularity distribute of 304 stainless steel

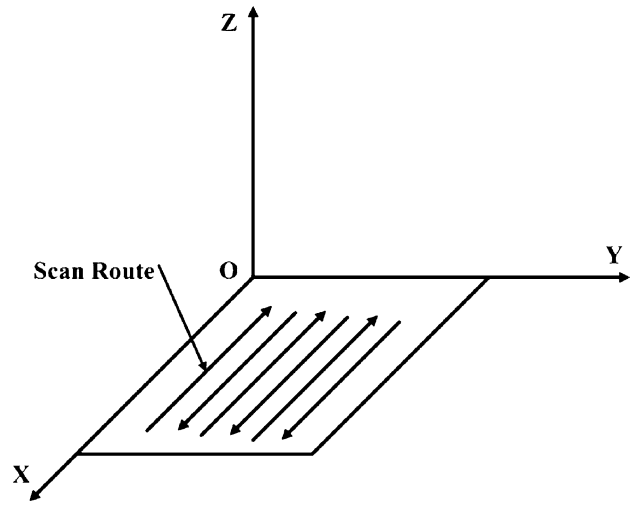

Fig. 2 The scan route of laser in SLS

2.2 Mechanical Experiments of Stainless Steel Metal Powder

To obtain some material properties used for simulation later, CIP experiments for the metal powder were required here. Stainless steel powder was poured into the cans made of paper to form column samples. These samples were tapped and sealed. Then, they were placed in the CIP device. Volumetric plastic strains and density of the samples were obtained under pressures of 100, 200, 300, 400, 450, and 630 MPa, respectively. The volumetric plastic strain is defined as $\varepsilon^{vp} = \varepsilon_{11} + \varepsilon_{22} + \varepsilon_{33}$, where ε_{11}, ε_{22}, and ε_{33} are the principal plastic strain of the samples.

The pressure versus volumetric plastic strain curve is plotted in Fig. 6. The fitted volumetric hardening curve in respect to least squares method is as function (1), p denotes hydrostatic pressure and ε^{vp} denotes volumetric plastic strain.

$$p = 18.86 \exp(6.41\varepsilon^{vp}) \quad \text{(Eq 1)}$$

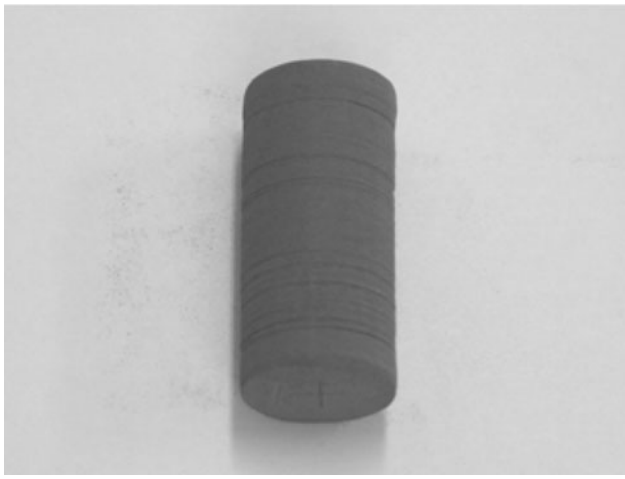

Fig. 3 The column sample after SLS

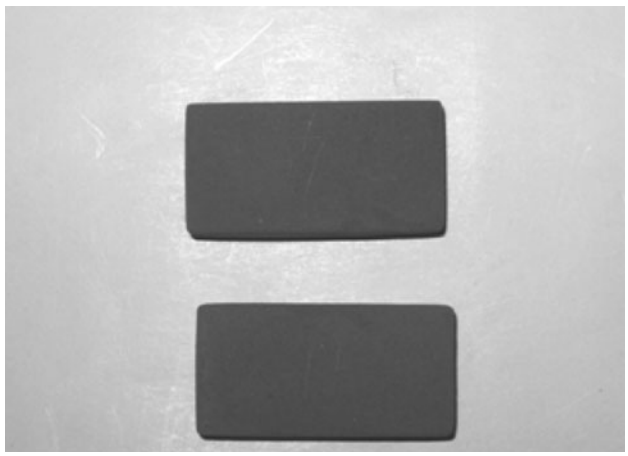

Fig. 4 The brick samples after SLS

Fig. 5 The parts after being coated by national rubber in outer surfaces

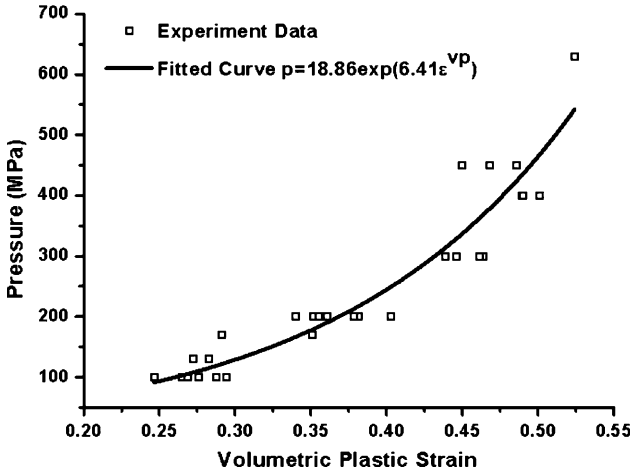

Fig. 6 Hydrostatic pressure vs. volumetric plastic strain (p is the pressure and is ε^{vp} the volumetric plastic strain)

3. Simulations

It is well known that the relative density of parts after SLS is low (about 30-40%) and after CIP can reach 70-80%. The dimensional changes associated with such increases in density are so large that in order to achieve a near net shape part, it is necessary to simulate the shape changes which occur during CIP.

3.1 Constitutive Equations

Metal powder is different from dense metal since for a dense metal, mass, and volume do not change after deformation. For metal powder, the volume will undergo permanent contraction and the density will increase under pressure. A modified Cam-Clay model (Ref 8) developed for soil plasticity can be used to describe the plastic yield of metal powder since the characteristics of metal powder are similar to those of soil.

The modified Cam-Clay model would be

$$F = \left(\frac{q}{M(p_0/2)}\right)^2 + \left(\frac{p - p_0/2}{p_0/2}\right)^2 - 1 = 0, \qquad \text{(Eq 2)}$$

where M is the degree of slope of critical state line, as shown in Fig. 7 and q is Mises stress, $q = \sqrt{3\boldsymbol{S_{ij}} : \boldsymbol{S_{ij}}/2}$, where $\boldsymbol{S_{ij}}$ is the deviatoric stress tensor. p is isostatic pressure. p_0 is parameter of volumetric hardening. It will increase with the pressure increment. Yield surface also has a tendency of expansion.

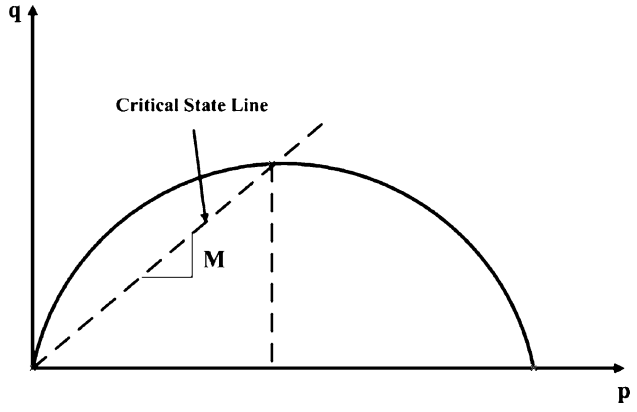

Fig. 7 The yield surface of modified Cam-Clay model on p-q plane (p is isostatic pressure, q is Mises stress, and M is the degree of slope of critical state line)

The stress-strain relation is now determined according to normal flow rule (Ref 9)

$$d\varepsilon_{ij}^{p} = d\lambda \cdot \partial F / \partial \sigma_{ij}, \qquad \text{(Eq 3)}$$

where $d\varepsilon_{ij}^{p}$ is the increment of plastic strain. $d\lambda$ is positive constant, and F is yield criterion.

The modified Cam-Clay model is incorporated in the normal flow rule. The relation of plastic strain increment and stress would be

$$d\varepsilon_{ij}^{p} = d\lambda \left[3S_{ij} \Big/ \left(M\frac{p_0}{2}\right)^2 + 2\left(p - \frac{p_0}{2}\right)\delta_{ij} \Big/ \left(\frac{9p_0}{2}\right)^2 \right], \qquad \text{(Eq 4)}$$

where δ_{ij} is Kronecker delta. Substituting Eq 4 into the yield criterion Eq 2 after some algebraic manipulations, the constant $d\lambda$ is obtained as Eq 5

$$d\lambda = \left[p_0 \sqrt{M^2 de_{ij}^{p} de_{ij}^{p}/6 + (d\varepsilon^{vp})^2/4} \right] \Big/ 2, \qquad \text{(Eq 5)}$$

where de_{ij}^{p} is the increment of deviatoric plastic strain.

3.2 Models

The models are an column (∅29.2 mm × 28.5 mm) shape and an brick (48.3 mm× 19.6 mm× 14.4 mm) shape, respectively. The column uses a four-node bilinear axisymmetric element while the brick uses an eight-node linear brick element. Because of the symmetry of the brick, only a quarter is used for analysis.

The simulations of CIP were carried out using finite element analysis. The stress-strain curve obtained in earlier experiments was used for material parameters. The parameter M is taken from Ref 10 as $M = 6.7$. Suppose that the modulus of elasticity is 200 GPa and do not change during the process and poison ratio is 0.3 (Ref 11). Because this paper focuses on the plastic deformation and the final dimensions, the elastic spring back is taken into account. Thus, the modulus of elasticity has little effect on the simulation results. The pressure applied was 650 MPa. Because the CIP process is carried out at room temperature, the effect of time on deformation is ignored. According to Ref 12 and 13, the gross shape of simulation gave a good agreement with the measured components except at the

corners if the effect of cans was not taken into consideration. Therefore, in this paper the influence of cans was not included.

3.3 Results of Simulation

The deformations of model in every direction are uniform as shown in Fig. 8 that accord to the experimental results. The comparisons of experiment and simulation after deformation are indicated in Table 2. The discrepancy of experimental measurements and simulations is within 4%. The origin of the disagreement may be the error in measurements of material properties and dimension measurements. The hardening law curve (as shown in Fig. 6) has been obtained by curve-fitting so it represents the average of strain at the specific pressure. Allowing for the error of numerical computation, the error of 4% is reasonable.

The plastic strains in *X*-axis in Fig. 9 are the same on the whole parts that implies the deformation is uniform under isostatic pressing condition. The shear plastic strain is not uniform on the whole parts as shown in Fig. 10. Its absolute values, however, are so small that is about an order of 10^{-7} that can be ignored. It implies the shear stress that leads to shear strain and further distortion of samples is very small. During CIP process, the samples are subject to the same pressure in all directions, so the principal stress of every point is equal and shear stress would be small. The contour of the relative density after unloading is shown in Fig. 11. The final relative density after CIP is 0.77 while that of simulation is 0.7677. A good accordance between the results of simulation and experimental results could be used to predict the final average density of the whole parts.

This results are different from those in reference (Ref 7) in that the parts were made from irregular powder and the shrinkage rate of the brick was big in the *Z* direction (about 19.8%; the directions are shown in Fig. 2) and that in other

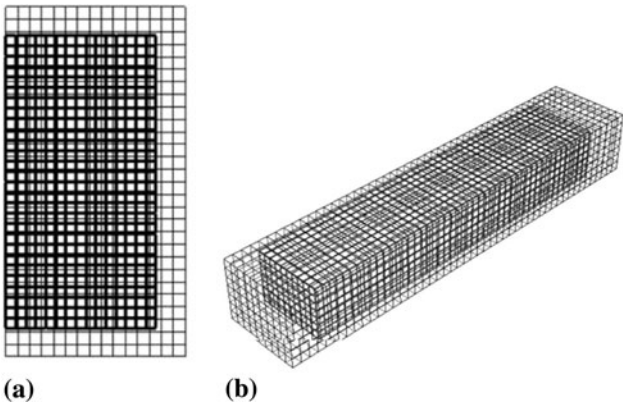

Fig. 8 The simulation results before and after cold isostatic pressing, slim lines denote the results before cold isostatic pressing, and *bold lines* denote the ones after cold isostatic pressing. (a) The simulation results of the column and (b) the simulation results of the brick

Table 2 Comparison of results of experiments and simulations

	Initial dimension	Results of experiments	Results of simulations	Relative error[a], %
Column				
Height	28.5	23.8	23.9	0.4
Diameter	29.2	23.8	24.4	2.5
Brick				
Length	48.3	40.8	40.4	−1.0
Width	19.6	16.6	16.4	−1.2
Height	14.4	12.5	12.0	−4.0

[a] Relative error = (simulation result − experiment result)/(experiment result)*%

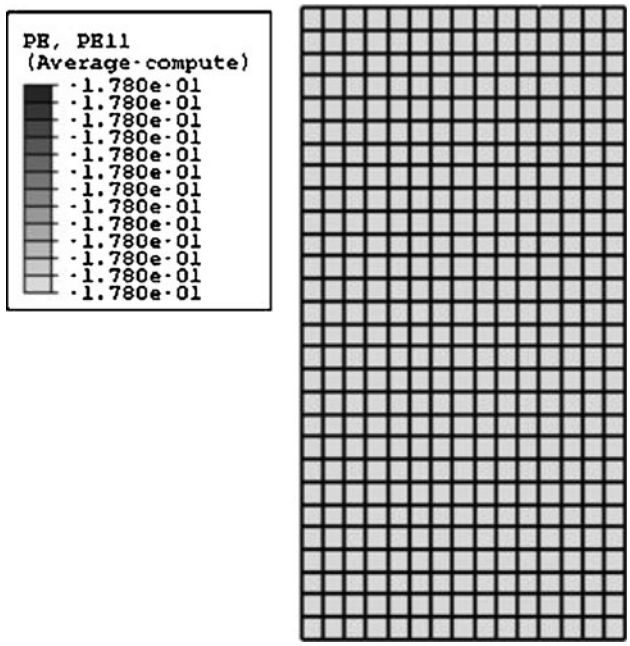

Fig. 9 The plastic strain contour of the column in *X* direction after unloading

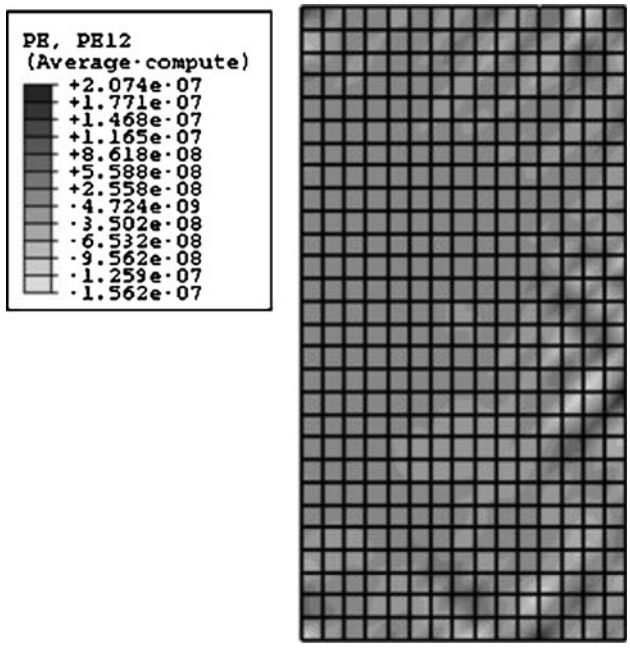

Fig. 10 The shear plastic strain contour of the column after unloading

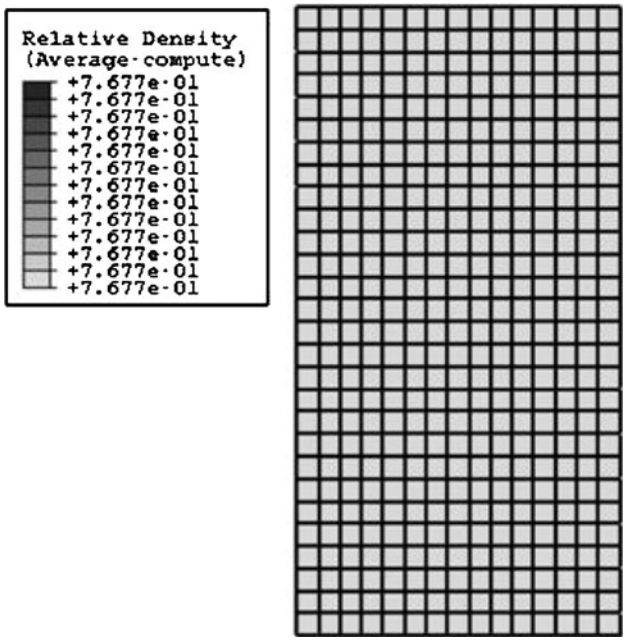

Fig. 11 The relative density contour of the column after unloading

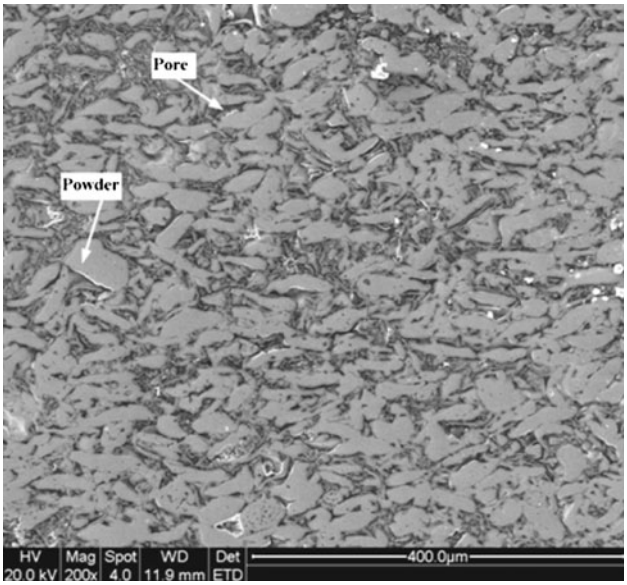

Fig. 12 The scanning electron microscope microscopic pictures of Fore-and-aft plane of the part of irregular powder after SLS

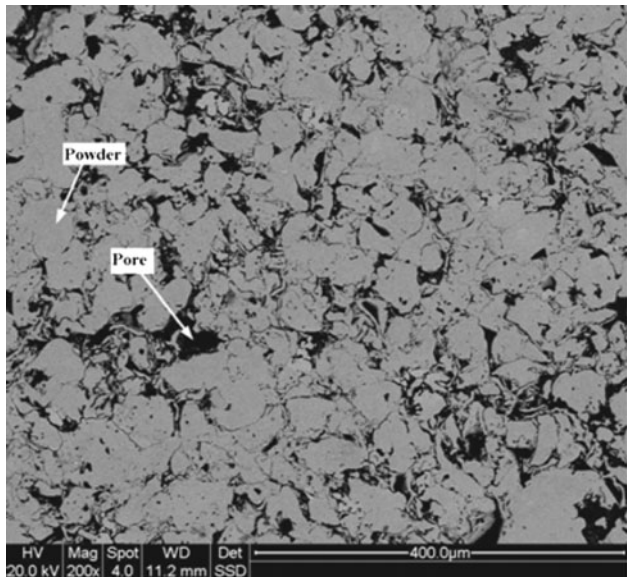

Fig. 13 The scanning electron microscope microscopic pictures of transverse plane of the part of irregular powder after SLS

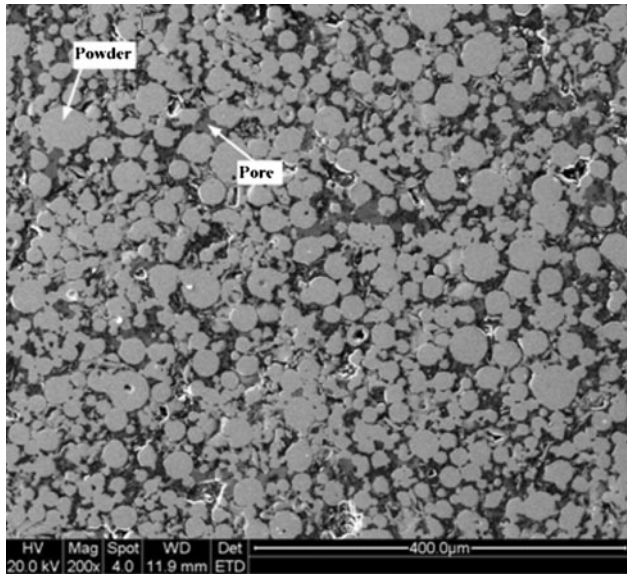

Fig. 14 The scanning electron microscope microscopic pictures of Fore-and-aft plane of the part of ball powder after SLS

directions was small (about 13%). The difference results from the specialty of SLS process and properties of the material as shown in SEM Fig. 12-15. The orientation of the irregular powder is very obvious in Fig. 12. In the transverse plane of Fig. 13, that is the build plane, there is no obvious orientation observed. There is also no orientation of powder obviously observed in Fig. 14 and 15 for spherical shape powder. Therefore, the shrinkages of the material are similar in all directions after CIP for spherical shape powder. However, the work reported in (Ref 7) has a bigger difference in Z direction.

Therefore, the spherical shape powder could make the parts shrink more uniform than irregular powder. It is also not easy to deform after CIP for the spherical shape. The accuracy of prediction results could decrease the cost of experiments and manufacture especially for more expensive CIP process and rare metal powder. It also supplies instructions for initial dimension design and forming technology such as forming pressure and final density of the parts.

4. Conclusions

It is feasible and practical that the metal components could be made by using SLS/CIP combined technology. The challenges of the process are the forming technologies of

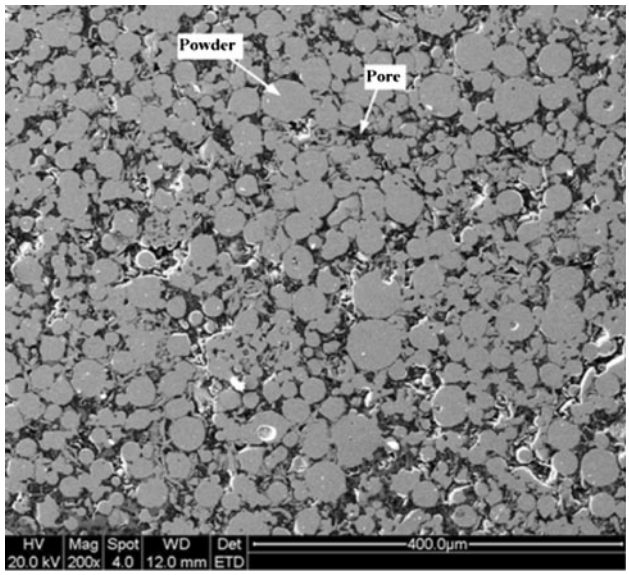

Fig. 15 The scanning electron microscope microscopic pictures of transverse plane of the part of ball powder after SLS

SLS and CIP and dimension error. A three-dimensional analysis of the model is also a challenge of the simulation. Only volume reduction occurred after CIP without shape torsion which is determined by the property of CIP and material. After CIP, the relative density of the parts could be increased to about 0.77. If more dense metal parts are required, HIP process should still be needed. The CIP process was simulated by making use of the Cam-Clay model. The results of simulation are compared with that of experimental measurements and a general agreement (better than 4%) is achieved. The simulation results could be used for dimension design to manufacture the near net shape parts. Future work will focus on the manufacture of more complex shapes parts and promotion of the prediction accuracy by achieving accurate material data and revising empirical model in order to supply useful constructions in dimension design of the part and forming process of CIP.

Acknowledgments

This research is funded by National 863 Project (2007AA03Z115) and Chinese Postdoctor Fund (20070410277). Appreciations are due to Doc. Lu Zhong Liang for his experiments of CIP and Prof. Wu Xin hua for revising the paper as well as Analytical and Testing Center of HuaZhong University of Science and Technology for SEM.

References

1. B. Odonnchadha and A. Tansey, A Note on Rapid Metal Composite Tooling by Selective Laser Sintering, *J. Mater. Process. Technol.*, 2004, **153-154**, p 28–34
2. J.P. Kruth, G. Levy, F. Klocke et al., Consolidation Phenomena in Laser and Powder-Bed Based Layered Manufacturing, *Ann. CIRP*, 2007, **56**(2), p 730–759
3. J.H. Liu, Y.S. Shi, Z.L. Lu et al., Manufacturing Near Dense Metal Parts via Indirect Selective Laser Sintering Combined with Isostatic Pressing, *Appl. Phys. A*, 2007, **89**, p 743–748
4. J.M. Torralba, E. Gordo, M.A. Jimenez et al., New Developments in Powder Technology, *Adv. Mater. Res.*, 2007, **23**, p 1–8
5. S.J. Mashl, Hot Isostatic Pressing of Particulate Materials, *Int. J. Powder Metall.*, 2005, **41**(5), p 45–55
6. M. Agarwala, D. Bourell, J. Beaman et al., Post-Processing of Selective Laser Sintered Metal Parts, *Rapid Prototyping J.*, 1995, **1**(2), p 36–44
7. Y.S. Shi, L.H. Ren, Q.S. Wei et al., Simulation of Cold Isostatic Pressing of Part by Selective Laser Sintering, *J. Huazhong Univ. Sci. Technol. (Nat. Sci. Ed.)*, 2007, **35**(12), p 91–94 (in Chinese)
8. K.H. Roscoe and J.B. Burland, On the Generalized Stress-Strain Behavior of "Wet" Clay, *Engineering Plasticity*, complied by J. Heyman and F.A. Leckie, Cambridge University Press, Cambridge, England, 1968, p 535–609
9. H.F. Chen, *Elasticity and Plasticity*, China Architecture and Building Press, BeiJing, 2003 (in Chinese)
10. X.K. Sun and Y.Y. Wang, Die Compaction Densification Behavior of Metal Powders, *Chin. J. Nonferrous Met.*, 1999, **9**(Suppl 1), p 239–241 (in Chinese)
11. F.W. James, *Materials Science and Engineering Handbook*, CRC Press, Boca Raton, 2001
12. R.J. Henderson, H.W. Chandler, A.R. Akisanya et al., Finite Element Modelling of Cold Isostatic Pressing, *J. Eur. Ceram. Soc.*, 2000, **20**(8), p 1121–1128
13. M. Reiterer, T. Kraft, U. Janosovits et al., Finite Element Simulation of Cold Isostatic Pressing and Sintering of SiC Components, *Ceram. Int.*, 2004, **30**(2), p 177–183